Hybrid Simulation of Waterwall and Combustion Process for a 600 MW Supercritical Once-through Boiler

Chen Yang[1], Hangxing He[2], Li Zhao[3]

Key Laboratory of Low-grade Energy Utilization Technologies and Systems, Ministry of Education of PRC,
College of Power Engineering, Chongqing University, Chongqing 400044, China
[1]yxtyc@cqu.edu.cn; [2]hhxkimi@cqu.edu.cn; [3]zhaoli_431@126.com

***Abstract*-This paper describes a hybrid simulation work on waterwall system and combustion process of a 600 MW supercritical boiler with W-flame furnace. A nonlinear distributed mathematical model which can be applied to the real time dynamic simulation was performed for analysing the dynamic characteristics of the waterwall system under typical working condition in this paper. The purpose of the numerical calculations was to determine the distributions of the fluid temperature and other corresponding thermal physical parameters. Coupled with the obtained fluid temperature as the boundary condition, the computational fluid dynamics (CFD) simulation of the combustion characteristics for the 600 MW supercritical boiler with W-flame furnace was conducted. Conventional methods usually separated the CFD simulations from process simulations; our work achieved the coupling between these two kinds of simulation. Through the hybrid simulation of these two models, more accurate distribution characteristics and combustion characteristics were obtained. The results reflect good agreements with the in-situ operating status of the supercritical boiler, which are valuable in practical engineering. And this work will be helpful for further design and research of the dynamic characteristics of the supercritical once-through boiler.**

Keywords- Supercritical Once-through Boiler; Distributed Parameter Model; W-flame Furnace; Hybrid Simulation

I. INTRODUCTION

A supercritical once-through boiler is an advanced power unit in the world with advantages of high thermal efficiency, low heat consumption compared to those of a subcritical boiler. In order to understand more clearly about the operational characteristics of a supercritical once-through boiler, numerical modeling of transient heat-flow processes and combustion characteristics occurring in the boiler has been raised and described in both domestic and foreign literatures [1-9].

The state of the fluid not only changes with the working conditions, but also changes over time. The heat-flow processes are nonlinear, and the nonlinearity results mainly from the dependency of thermophysical properties of the fluid. As for the investigation of combustion characteristics, researchers tended to implement the simulation with boundary conditions of constant wall temperature, but these sources of wall temperature datum were mostly not pointed out [10]. The hydrodynamic characteristics of waterwalls play extremely important roles in reflecting the combustion characteristics. Moreover, the hybrid simulation of furnace combustion model and waterwall system is rare among all the references. Therefore, a hybrid simulation is carried out in this paper.

In this paper, a nonlinear distributed mathematical model is applied for the analysis of the flow and heat transfer processes occurring in the waterwalls of the supercritical boiler [11]. The purpose of the numerical calculations is to determine the distributions of the fluid temperature and other corresponding thermal physical parameters. And then the obtained fluid temperature distribution is used as the boundary condition of the computational fluid dynamics (CFD) simulation which is implemented with Fluent 6.3. This paper studies both the fluid heat-flow characteristics of the waterwall and the furnace combustion processes, makes the hybrid collaborative simulation come true. This method overcomes the deficiency of previous researches with two isolated models and improves the accuracy and authenticity of the simulation results for boilers.

II. DESCRIPTION OF THE OBJECT

The object of the hybrid simulation is a 600MW supercritical unit with W-flame furnace of Dongfang Boiler Group Co. Ltd. The boiler, type of Dongfang DG1950/25.4- II8 is being used in Sichuan Gongxian, China. This type of boiler is designed for supercritical parameters with W-flame furnace and vertical waterwall pipes. In this paper, using the ratio of 1:1for the actual model and the calculation model. Due to the symmetry of the furnace structure, taking only a half of the furnace structure for investigation. The geometrical structure of the furnace and the main parameters are shown in Fig. 1 and Table 1, respectively.

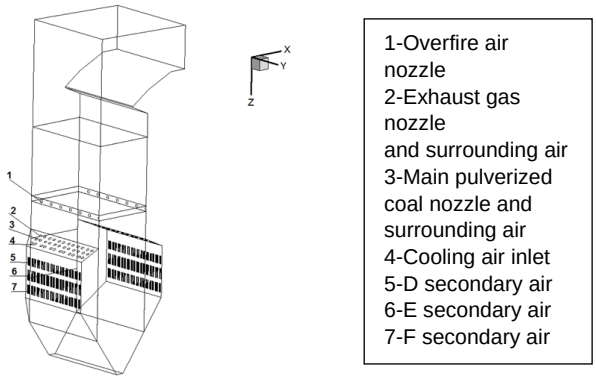

Fig. 1 Geometrical model of the furnace

TABLE 1 THE CAPACITY AND MAIN PARAMETERS OF THE BOILER

	Unit	BMCR	BRL	THA
Superheated steam flow rate	kg/s	541.7	511.3	471.6
Pressure of superheater outlet	MPa(g)	25.7	25.33	25.15
Temperature of superheater outlet	K	845	845	845
Reheat steam flow rate	kg/s	441.9	416.3	388.4
Pressure of reheater inlet	MPa(g)	4.74	4.46	4.17
Pressure of reheater outlet	MPa(g)	4.56	4.28	4.0
Temperature of reheater inlet	K	598	591	585
Temperature of reheater outlet	K	843	843	843
Temperature of economizer inlet	K	562	558	553

III. MATHEMATICAL MODEL

A. Waterwall Model with Distributed Parameters

The waterwall system of a boiler has features of nonlinearity and distributed parameters, so the nonlinear distributed parameter model is built to simulate the transient heat-flow processes occurring in the heated surfaces of the power boiler.

The mathematical model is mainly composed of a set of partial differential equations. These equations and corresponding algebraic equations constitute the basic mathematical model. High precision results can be obtained with the nonlinear distributed model combined with the actual operation conditions.

As it is difficult to obtain the boundary conditions of the furnace during the actual operation, the one-dimensional model of the waterwalls, established in this paper, can provide the required temperature boundary conditions for the simulation of furnace combustion. The model is based on the solution of equations describing the conservation laws of mass, momentum and energy. The control volume (CV) of the waterwall is shown in Fig. 2. The following equations are based on the analysis of the CV.

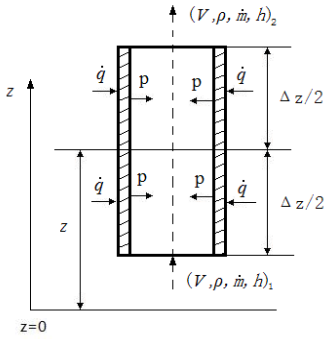

Fig. 2 Control volume of waterwall

To simulate the heat and flow processes in continuous medium, these differential forms of the mass, momentum and energy conservation equations are used [11].

Mass conservation equation:

$$\frac{\partial \rho}{\partial \tau} = -\frac{1}{A}\frac{\partial \dot{m}}{\partial z} \tag{1}$$

Momentum conservation equation:

$$\frac{\partial \dot{m}}{\partial \tau} = -\frac{1}{A}\frac{\partial}{\partial z}\left(\frac{\dot{m}^2}{\rho}\right) - A\left(\frac{\partial p}{\partial z} + \frac{\partial p_\tau}{\partial z} + \rho g\right) \tag{2}$$

In the momentum equation, momentum of inflow and outflow flux and the rate of momentum accumulation in the CV are taken into consideration. The surface and mass forces are also taken into account.

Energy conservation equation:

$$\frac{\partial h}{\partial \tau} = \left(1 - \frac{1}{\rho}\frac{\partial p}{\partial h}\right)^{-1}\left[\frac{\dot{m}}{A\rho}\left(\frac{1}{\rho}\frac{\partial p}{\partial z} - \frac{\partial p}{\partial h} + \frac{1}{\rho}\frac{\partial p_\tau}{\partial z}\right) + \frac{4\alpha(\theta - t)}{d_{in}\rho} - \frac{1}{A\rho}\frac{\partial p}{\partial \rho}\frac{\partial \dot{m}}{\partial z}\right] \tag{3}$$

Surface forces and the energy carried out by the volume are omitted in Eq. (3).

There are many empirical formulae to calculate the heat transfer coefficient. For the calculation of the heat transfer coefficient at overcritical pressures, the Kitoh formula [12] is used in this paper:

$$Nu = 0.015\,\mathrm{Re}_f^{0.85}\,Pr_f^m \tag{4}$$

Where

$$m = 0.69 - \frac{81000}{q^*} + f_c\dot{q}, q^* = 200G^{1.2} \tag{5}$$

$$\begin{cases} 29\times10^{-8} + \dfrac{0.11}{q^*}, 0 \le h_f \le 1500kJ/kg, \\ -8.7\times10^{-8} - \dfrac{0.65}{q^*}, 1500 \le h_f \le 3300kJ/kg, \\ -9.7\times10^{-7} + \dfrac{1.3}{q^*}, 3300 \le h_f \le 4000kJ/kg. \end{cases} \tag{6}$$

To solve Eq. (1), (2) and (3), the implicit difference method was used [11]. The spatial derivatives are substituted by backward difference scheme and the time derivatives are substituted by forward difference scheme.

All thermophysical properties of the fluid are computed by the program of steam properties functions in real-time [13]. Along with essential constitutive equations, the model of waterwall system is completely built. Applying these difference schemes, the distributions of the mass flow rate, pressure and enthalpy of the fluid can be determined. And further to obtain the distributions of temperature of the fluid and waterwall tubes, as well as some other properties of the fluid.

B. Mathematical Model of Combustion in the Furnace

The pulverized coal particles are considered as discrete phase and the gas flow is calculated as continuous medium. The detailed models are described as follows.

1) Turbulent Flow Model

The standard k-ε model was applied for the simulation of turbulent flow in the furnace [14], described as follows:

k equation:

$$\frac{\partial k}{\partial t} + \overline{u_k}\frac{\partial k}{\partial x_k} = -\frac{\partial}{\partial x_k}\overline{[u_k'(\frac{p'}{\rho} + \frac{1}{2}u_i'u_i')]} - \overline{u_i'u_k'}\frac{\partial \overline{u_i}}{\partial x_k} + \nu\frac{\partial^2 k}{\partial x_k \partial x_k} - \nu\frac{\partial \overline{u_i}}{\partial x_k}\frac{\partial \overline{u_i}}{\partial x_k} \tag{7}$$

ε equation:

$$\begin{aligned} \frac{\partial \varepsilon}{\partial t} + \overline{u_j}\frac{\partial \varepsilon}{\partial x_j} = {} & -2\nu u_j'\overline{\frac{\partial u_i'}{\partial x_j}\frac{\partial^2 u_j'}{\partial x_j \partial x_k}} - 2\nu^2\overline{\frac{\partial^2 u_i'}{\partial x_k \partial x_j}\frac{\partial^2 u_i'}{\partial x_k \partial x_j}} + \frac{\partial}{\partial x_j}[\nu\frac{\partial \varepsilon}{\partial x_j} - \nu u_k'\overline{\frac{\partial u_i'}{\partial x_j}\frac{\partial u_i'}{\partial x_j}} - \frac{2\nu}{\rho}\overline{\frac{\partial u_j'}{\partial x_k}\frac{\partial p'}{\partial x_k}}] - \\ & -2\nu\overline{\frac{\partial u_i'}{\partial x_k}\frac{\partial u_j'}{\partial x_k}\frac{\partial u_i'}{\partial x_j}} - 2\nu\frac{\partial \overline{u_i}}{\partial x_k}(\overline{\frac{\partial u_i'}{\partial x_j}\frac{\partial u_i'}{\partial x_j}} + \overline{\frac{\partial u_k'}{\partial x_j}\frac{\partial u_k'}{\partial x_i}}) \end{aligned} \tag{8}$$

2) The Gas-Particle Two-Phase Flow Model

The motion of pulverized coal particle is a typical gas-particle two-phase flow, and it is analysed based on particle orbital model. The force balance equation of particles in x direction can be calculated as [15]:

$$\frac{du_p}{dt} = F_d\left(u-u_p\right)+\frac{g_x\left(\rho_p-\rho\right)}{\rho_p}+F_x \tag{9}$$

Where $F_d(u\text{-}u_p)$ represents mass drag force of particles, F_x represents the additional mass force:

$$F_d\left(u-u_p\right)=\frac{18\mu}{\rho_p d_p^2}\frac{C_d\,\mathrm{Re}}{24}\left(u-u_p\right) \tag{10}$$

$$F_x=\frac{1}{2}\frac{\rho}{\rho_p}\frac{d}{dt}\left(u-u_p\right) \tag{11}$$

The particle orbital equations:

$$x_p=\int u_p dt,\quad y_p=\int v_p dt,\quad z_p=\int w_p dt \tag{12}$$

3) Combustion Model of Pulverized Coal

Combustion model consists of coal particle pyrolysis, pulverized coal volatile combustion and char combustion. As the combustion progresses, the temperature of coal particles began to change:

$$\frac{d}{dt}\left(m_p c_p T_p\right)=h_c A\left(T_f-T_p\right)+H_v m_i\frac{dv}{dt}+H_c Aq \tag{13}$$

The single-reaction model is established for the analysis of coal pyrolysis [16]; the particle pyrolysis rate follows the Arrhenius chemical reaction rate:

$$\frac{dv}{dt}=k\left(v_\infty-v\right) \tag{14}$$

Then, mixture fraction probability density function (PDF) model was used to the simulation of pulverized coal volatile combustion model and the diffusion kinetic model was applied for char combustion [17].

4) Radiant Heat Transfer

Since the heat transfer between the heating surface and the products of combustion is mainly caused by thermal radiation, therefore the selection and settings for the radiation model is essential for numerical simulation of the furnace. P1 method was selected for calculations of radiant heat transfer, wall boundary condition of the radiant heat flux q_r can be expressed as:

$$q_{r,w}=\frac{\varepsilon_w}{2(2-\varepsilon_w)}\left(4\sigma T_w^4-G_w\right) \tag{15}$$

5) Nitrogen Oxide Generation

NO_x consists of several nitrogen-oxygen compounds. For a coal power plant, the nitrogen oxides generated during the combustion process in the furnace are mainly composed of nitrogen monoxide. Therefore, only nitrogen monoxide production is taken into consideration in the numerical calculations for nitrogen oxide generation. Post-processing method is used to simulate the generation of nitrogen monoxide. The reaction mechanism of nitrogen monoxide is shown in Fig. 3:

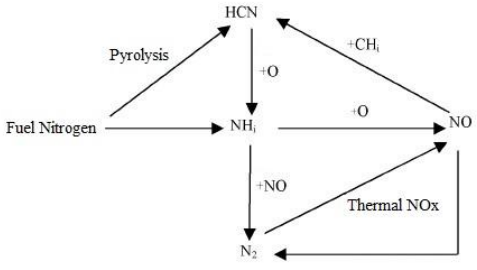

Fig. 3 Reaction mechanism of NO

In this paper, using software package Fluent as the platform for the numerical simulation of combustion processes, models of different objects in the furnace are summarized as follows [18]: the standard k-ε model for the turbulent flow, mixture fraction probability density function (PDF) model for volatile combustion, diffusion kinetic model for char combustion, a single-reaction model for the pyrolysis analysis, stochastic orbital model for gas-particle two-phase flow, P1 model for radiant heat transfer, the standard wall function for near-wall treatment and combustion post-processing method for generation of nitrogen oxides.

C. Mesh Generation

The structures of supercritical W-flame boilers are complex with a lot of irregular geometries, therefore a mixed meshing method including structured and unstructured grid is employed. The number of the grids is around 850,000. For upper combustion chamber and the ash hopper at the bottom coupled with other areas with relatively regular geometries, the flow, heat transfer phenomena and chemical reactions are simple. Sparse structured grids are generated in these areas. On the contrary, the heat and flow processes and chemical reactions are complicated in the areas of overfire air and lower combustion chamber, so precise unstructured grids are used. Meshing is basically consistent with the flow direction, it allows effective reduction of the false diffusions in numerical simulations, see Fig. 4.

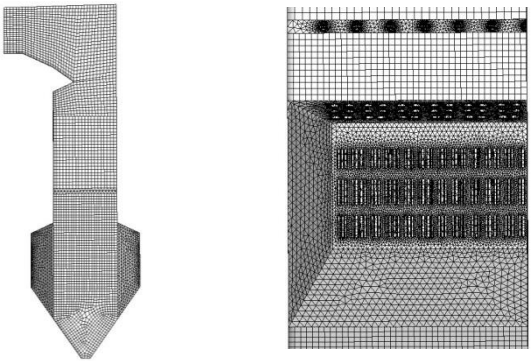

Fig. 4 The grid map of the furnace

D. Boundary Conditions

According to the temperature distribution calculated in the waterwall model, the corresponding furnace temperature boundary can be obtained. Different heights of the furnace are setting by sections, where the walls with refractory lining are setting for adiabatic boundary condition.

Velocities of the inlets are used as the boundary conditions in the burner, primary and secondary air. The pressures of the outlets are set as boundary conditions for the outlets. The settings are shown in Table 2.

TABLE 2 DESIGN PARAMETERS AT BOILER INLETS

	Velocity/m·s^{-1}	Temperature/K	Fuel Consumption/kg·s^{-1}
Main nozzle	28	388	1.5
Surrounding air of main nozzle	39	622	
Exhaust gas nozzle	11.5	388	0.167
Surrounding air of exhaust gas	40	622	
Cooling air	13	622	
Straight flow of overfire air	45	605	
Rotational flow of overfire air	34	622	
D secondary air	1	622	
E secondary air	1	622	
F secondary air	14.5	622	

IV. RESULTS AND ANALYSIS

A. Numerical Results under Typical Working Condition

When the boiler is running at THA (Turbine Heat Acceptance) load, the pressure of water separator will be 26.97MPa, the

feedwater mass flow rate reaches 471.6kg/s and the initial temperature of feedwater is 553K. As the model calculation steps, $\Delta\tau$ = 0.04 s and Δz = 0.5 m for the waterwall model were applied to avoid dissipation and dispersion at the grids. The computational results obtained in the selected cross-sections are shown in Figs. 5-9. These results obtained in present work are consistent with the calculations presented by Zima [11] with the assumed calculation data (water pressure at the waterwall inlet is 30Mpa; mass flow rate is 555.6kg/s; supplied water temperature at the inlet is 563K).

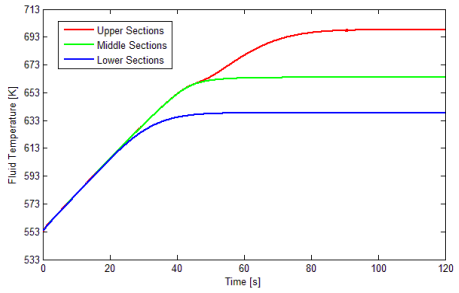

Fig. 5 Histories of fluid temperature

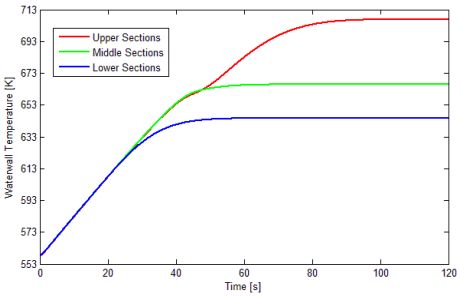

Fig. 6 Histories of temperature of waterwll tube

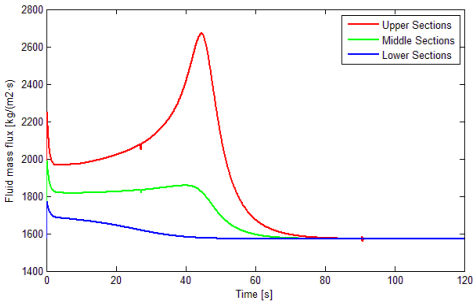

Fig. 7 Histories of fluid mass flux

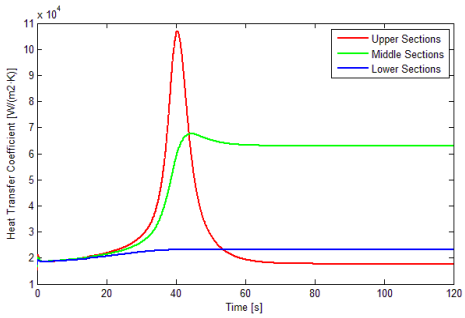

Fig. 8 Histories of the heat transfer coefficient

Figs. 5-8 indicate completely satisfactory of the results obtained by the distributed parameter model. Fig. 5 and Fig. 6 show the distributions of fluid temperature and waterwall tube temperature with respect to time, respectively. From these figures, it is can be seen that the maximum recommended design metal temperature is not exceeded. The temperature is 823K and 778K respectively for 12CrMoV and 15CrMoG steel. Fig. 7 shows that fluid mass flux reaches the level recommended for once-through boilers. Histories of the heat transfer coefficient in selected cross-sections are shown in Fig. 8 as an example of the thermophysical properties computed in the real-time.

In order to obtain the boundary conditions for the simulation of combustion processes in the furnace, the temperature distributions of waterwall tube are carried out, see Fig. 9.

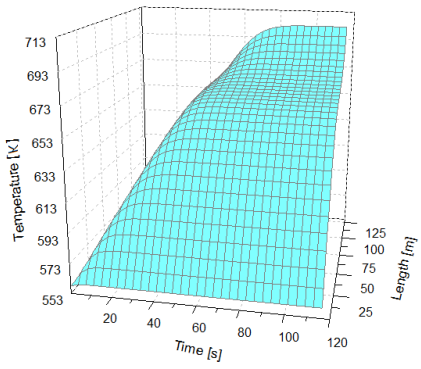

Fig. 9 Temperature distribution of waterwall tube

The numerical results of combustion characteristics are shown in Figs. 10-12. Representative longitudinal sections: Y=15.37 m (about 1/2 of the furnace depth), Y=8.647 m, Y=4.165 m, Y=0 m (side wall) are taken for the analysis of distributions of combustion characteristics in the furnace.

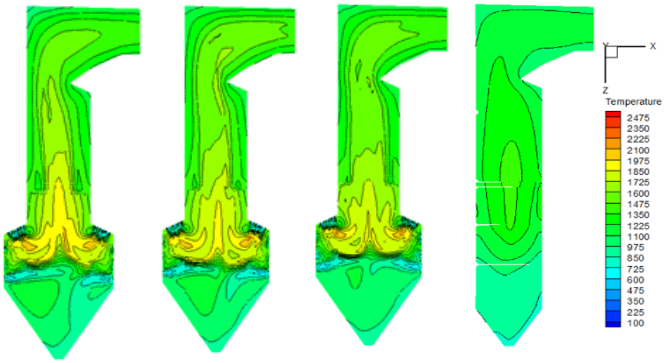

Y=15.37 Y=8.647 Y=4.165 Y=0

(a) Distributions of temperature field at different depth

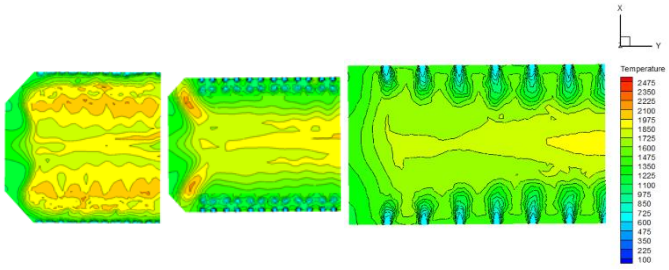

Z=9.9 Z=7.2 Z=1.29

(b) Distributions of temperature field at different height

Fig. 10 Distributions of temperature field in the furnace (unit: K)

Fig. 10(a) shows that the flame satisfied a good degree of fullness in the burner region. The temperature under the arch is high, which is conductive to sustain the ignition and stabilization of the pulverized coal combustion. But it reaches the deformation temperature (1383K) designed for coal ash in these areas, coupling with vortexes on the waterwall, the probability of coking on the surfaces increases. Temperature near the overfire air nozzles could also be as high as the deformation temperature. Once the overfire air is injected to supplement further oxygen needed by coal combustion timely, it can help reducing the probability of slagging at the wall surface. Degrees of burning flame are weakened from the central to the side wall area, and the proportion of high-temperature flame reduces, too. The maximum temperature reaches 2475 K, obtained

under the arch where the burning is exuberant.

Fig. 10(b) shows the distributions of temperature of cross-sections at different heights in the furnace. Combustion in the region of secondary air is exuberant because of sufficient oxygen supplement. In parallel this could easily lead to the generation of NO_x pollutants. By the observation of temperature distributions around the exhaust gas wind area, a high-temperature vortex is generated at the wing region close to the side wall. It provides favourable conditions for slagging, which happens a lot during the actual operating conditions.

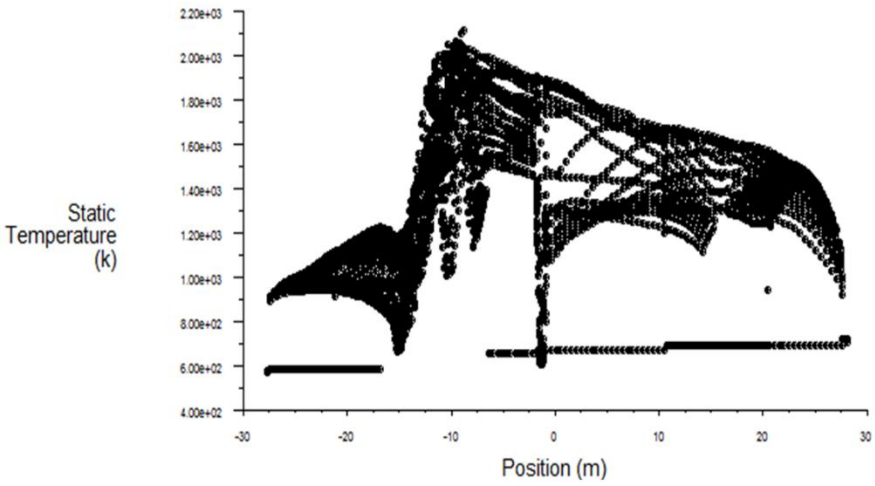

Fig. 11 Distributions of temperature along the height at central section of the furnace (unit: K)

Shown in Fig. 11, the temperature increases along the furnace height and reaches the maximum value in the combustion zone. Then, it began to decline. Temperature at the outlet of furnace is 1315.16 K, while the design value of this boiler type is 1279 K. So the error is 2.83%, which indicates good agreements with the design conditions.

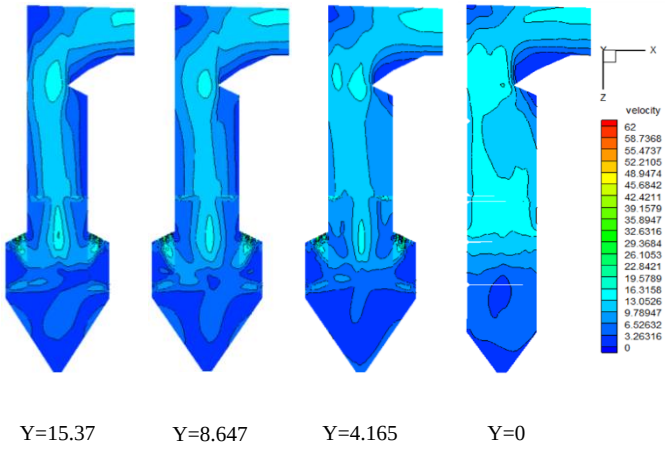

Fig. 12 Distributions of flow field at different depth of the furnace (unit: $m \cdot s^{-1}$)

The distributions of the flow field in the furnace are shown in Fig. 12, with a distinct shape of W-flame. A strong vortex is formed near the primary air nozzle. High-temperature gas entrainments reinforce the stability of pulverized coal combustion. Areas under the arch and the central part of the furnace are at high flow velocities because of the rapid expansions of high-temperature air.

In the burner zone, the flow shape "W" is getting weakened and the average velocities decrease from the central part to the side wall gradually. This is caused by rapid expansions of the high-temperature fuel gas in the central part of the furnace. The asymmetry of distributions between the front wall and rear wall could lead to coking and even pipe explosion.

The distributions of gas component concentrations along the height of furnace are shown in Fig. 13. There is a significant relevance between furnace temperature and the concentrations of O_2 and CO_2. The concentration of O_2 is relatively low in the area of exuberant burning, in addition, the concentration of O_2 changes rapidly in these areas. The distribution of CO_2 concentration in the furnace is just the opposite to that of O_2. From the observation of CO mass concentration, the formation of CO is more likely to be happened at the junction where the concentrations of CO_2 and O_2 change dramatically. Due to the supplement of sufficient oxygen at overfire air region, almost the entire CO in the vertical shaft is converted into CO_2.

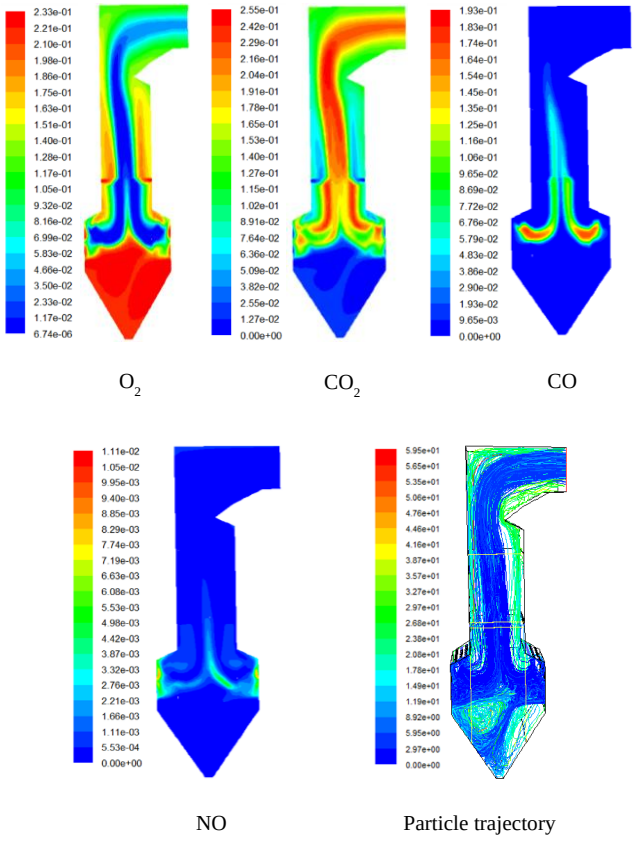

Fig. 13 Distribution of component concentrations and particle trajectory in selected sections

Fig. 13 also exhibits the generation of NO and the distribution of its concentration. Since the vortex is not completely diffusion, an annular region with high concentration of NO is formed near the wall. The temperature under the arch keeps rising up as the combustion progresses, which promotes the reactions of nitrogen atoms and oxygen. Then, the generated NO spreads to the central areas continuously.

Coal particles, driven by high-temperature gas, mainly distribute in the opposed firing regions of the lower combustion chamber and in the central areas of the upper furnace. The trajectory presents a biased asymmetry towards the front wall, which could easily lead to heat transfer deterioration and non-uniformed heating of the waterwall tubes. Therefore, the probability of heat transfer deterioration is higher at the front wall.

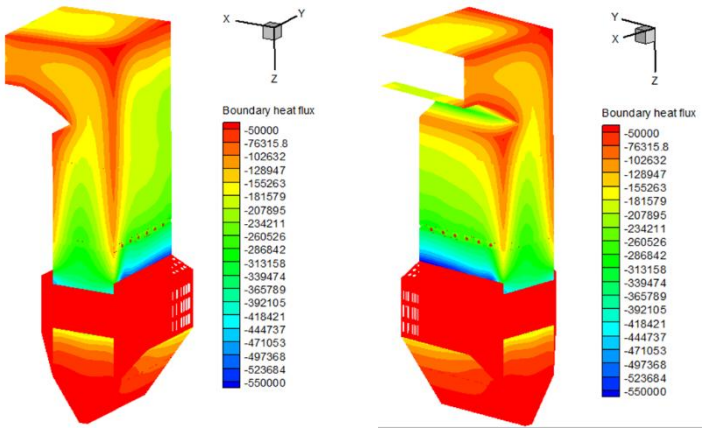

Fig. 14 Contours of heat transfer coefficients at wall surface ($W/m^2 \cdot k$)

Fig. 14 shows the contours of heat transfer coefficients at wall surface. The values are negative because combustion chamber is in the process of releasing heat. Heat exchange in the furnace is dominated by radiation, the high-temperature areas have high heat transfer coefficients and the gradients change obviously in these areas. The heat transfer coefficients reach the highest value between the burner zone of the front and rear wall and overfire-air zone. Due to the existence of the furnace arch, the heat transfer coefficients change dramatically near the arch, therefore it provides favourable conditions to cause

non-uniformed heating of waterwall pipes.

B. Numerical Results under Different Conditions

Numerical simulation was conducted at THA, 75% THA and 50% THA loads, respectively. Figs. 15-17 show the distributions of parameters at the cross-sections of the central part of the furnace under three different conditions.

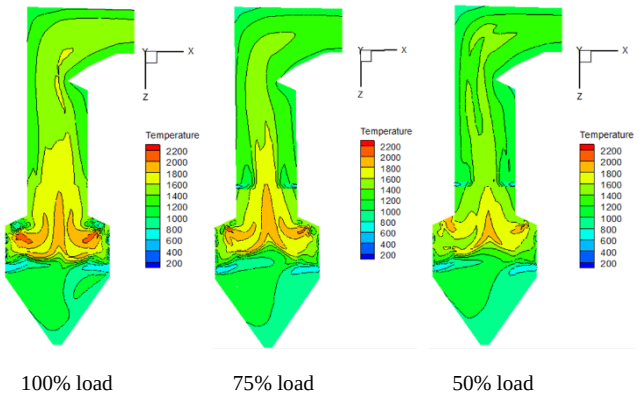

Fig. 15 Distributions of temperature field under different conditions (unit: K)

Fig. 15 shows the distributions of temperature at the selected cross-sections. The high-temperature area (T>1800K) with W-flame becomes small along with the reduction of thermal loads gradually; in parallel the asymmetry of the flame is increasingly obvious.

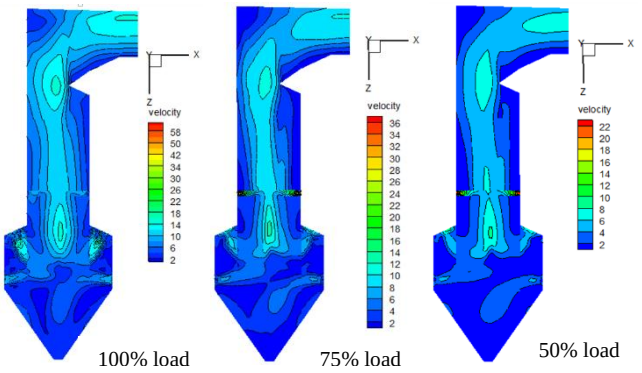

Fig. 16 Distributions of flow field under different conditions (unit: $m \cdot s^{-1}$)

Fig. 16 shows the distributions of flow at the cross-sections. Low-velocity regions increase gradually with the reduction of thermal load in the furnace. The range of velocity is in the order of 0~56 m/s, 0~36 m/s and 0~22 m/s under the three different conditions.

With the reduction of the load, the average temperature and the gas velocity decrease. High temperature and the scour by gases could lead to coking on the wall surface, therefore the boiler walls are more likely to be coking at high thermal load conditions. This is consistent with the actual situations. Because of the reduction of high-temperature region, the rate of coke combustion is limited; as a result, the fuel utilization is incomplete.

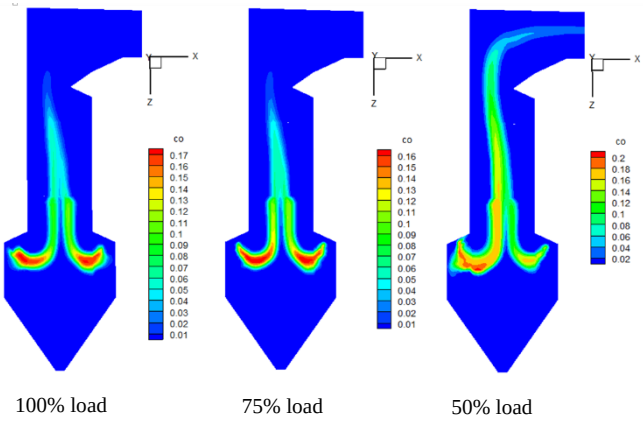

Fig. 17 Profiles of mass fraction of CO under different conditions

As shown in Fig. 17, the proportion of CO generated in the furnace and at the outlet is large when working at low loads. Plenty of CO is generated at 50% THA load; there still exists some CO gas at the outlet of furnace. By contrary, the CO gas generated at high loads has been converted into CO_2 sufficiently.

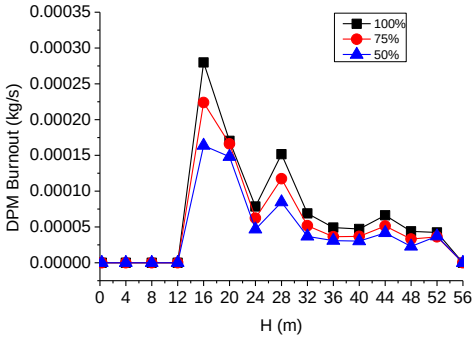

Fig. 18 Histories of the average cross-sectional combustion ratio of pulverized coal

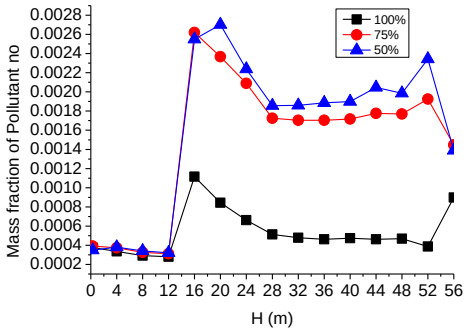

Fig. 19 Histories of the average cross-sectional concentrations of NO

Fig. 18 shows the combustion ratio changing with the height of furnace. Values of the combustion ratio reach the maximum at the lower furnace where the secondary air is sufficient. The values under high load are higher than that under low load.

Fig. 19 shows the average cross-sectional concentrations of NO. When the furnace is under full load, the concentration of NO along the furnace height was firstly increased and then decreased and increased again. When working under 75% or 50% thermal load, after the value of concentration increased again, it will decrease afterwards. The concentration of 75% load and 50% load are much higher than the concentration of NO under full load. The maintenance of the boiler operation under high thermal loads is benefit to reduce the emissions of nitrogen oxide.

C. Numerical Results of Variable Load Transient Simulation

According to numerical results obtain by the waterwall model; we investigated the effect of waterwall tube temperature change on combustion dynamics in the furnace. Use UDF macro function to achieve the simulation of variable load transient process in occurring in the furnace. The load transient process is set to change from 75% THA to 90% THA. The PISO

algorithm, which is suitable for solving non-steady-state problems, is employed for the simulation. The time step, $\Delta t = 0.005$ s, is set for the numerical calculations.

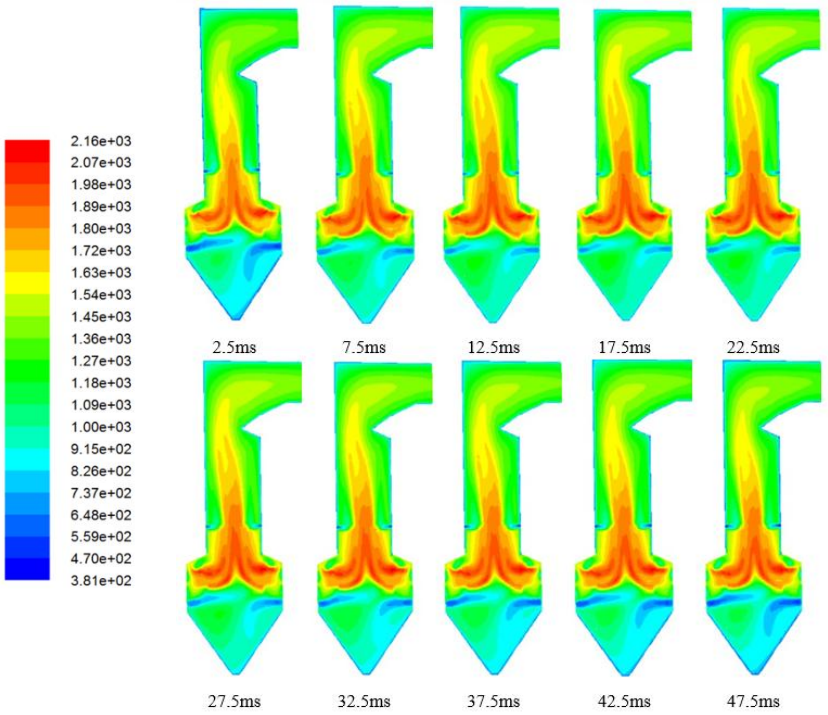

Fig. 20 Histories of temperature field in the furnace (unit: K)

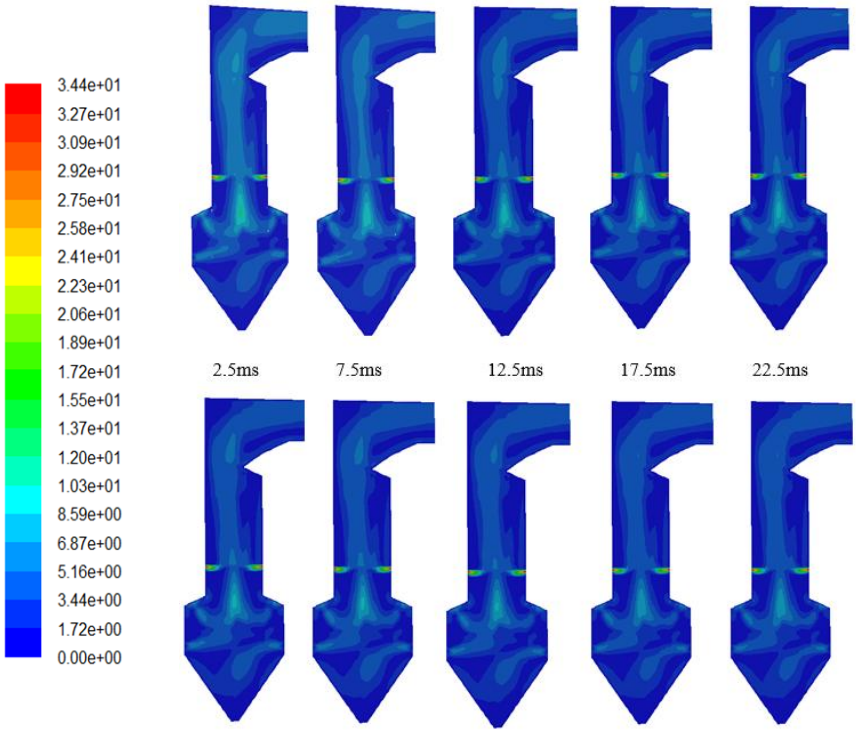

Fig. 21 Histories of flow field in the furnace (unit: $m \cdot s^{-1}$)

Figs. 20 and 21 show the temperature and flow field changes during the trans-critical process. The calculation time in the furnace lasts 47.5ms; wall temperature and the thermal load are set to maintain a fixed value after 36ms. The combustion becomes exuberant with the increasing load; when the transient processes come to an end, as the heat transfer between the air flow and the waterwall tube continues, the combustion decays gradually. The flow field shows tiny variations in the burner

zone; the high-velocity area is slightly reduced in the upper furnace. Although the thermal load, the amount of inlet air and fuel injecting rate are increasing, the influence on the entire furnace flow conditions is slight from 75% THA to 90% THA. Therefore, the trans-critical process in the waterwall pipes will not cause serious effects on the stability of the combustion in the furnace.

V. CONCLUSIONS

In this paper, a nonlinear distributed mathematical model is applied for the analysis of the flow and heat transfer processes occurring in the waterwalls of the supercritical boiler. The determination of thermophysical properties of the fluid in the waterwalls is of great importance for the accuracy of the obtained temperature distributions. The temperature distributions are used as boundary conditions for the simulation of combustion characteristics. Compared to other literatures, the results obtained by the hybrid simulation in this paper are more persuasive.

Results of the combustion characteristics in the furnace show great consistency with the actual operation of the boiler. The asymmetry of the distributions of the flow field, the temperature field and pulverized coal particle trajectory indicate that, it is likely to cause slagging by high-temperature scour near the front wall, side walls and wing walls. Therefore, it is necessary to strengthen the blowing in these areas. When working under high loads, it is easily to cause coking but the symmetry and fullness of the flame are of good values for the burnout of coal particles. The reduction of probabilities of slagging and the reduction of the amount of nitrogen oxides are mutually contradictory; it can be optimized by adjusting the amount of air and pulverized coal needed for combustion. As a consequence, through the hybrid simulation of the supercritical once-through boiler, the results reflect good agreements with the in-situ operating status of the supercritical boiler, which are valuable in practical engineering. And this work will be helpful for further designs and researches of dynamic characteristics of supercritical once-through boilers.

ACKNOWLEDGMENT

The authors gratefully acknowledge the support of the National Nature Science Foundation of China (No. 50876117).

REFERENCES

[1] Z. H. Wang and J. G. Meng, "Analysis of Development Status of Supercritical W-shaped Flame Boiler in China," *Electric Power Construction*, vol. 28, no. 9, pp. 65-69, 2007 (in Chinese).

[2] J. Taler and P. Duda, *Solving Direct and Inverse Heat Conduction Problems*, Berlin: Springer, 2006.

[3] H. B. Lu, Y. Zhang, C. K. Wu, and W. H. Sun, "Dynamic Model Identification of the Main Steam Temperature for Supercritical Once-through Boiler," *Energy Procedia*, vol. 17, pp. 1704-1709, 2012.

[4] S. Zheng, Z. X. Luo, X. Y. Zhang, and H. C. Zhou, "Distributed Parameters Modeling for Evaporation System in a Once-through Coal-fired Twin-furnace Boiler," *International Journal of Thermal Sciences*, vol. 50, p. 2496-2505, 2011.

[5] Z. Y. Gao, W. Song, and J. Zhao, "Numerical Simulation of the Combustion Characteristics of the W-flame Boiler under Different Loads," *Journal of North China Electric Power University*, vol. 37, pp. 63-67, 2007 (in Chinese).

[6] W. Zima, "Simulation of Dynamics of a Boiler Steam Superheater with an Attemperator," Proc. of the Institution of Mechanical Engineers, Part A: *Journal of Power and Energy*, pp. 793-801, 2006.

[7] X. J. Liu, X. B. Kong, G. L. Hou, and J. H. Wang, "Modeling of a 1000MW Power Plant Ultra Super-critical boiler system using fuzzy-neural network methods," *Energy Conversion and Management*, vol. 65, pp. 518-527, 2013.

[8] J. Pan, D. Yang, H. Yu, Q. C. Bi., H. Y. Hua, F. Gao, and Z. M. Yang, "Mathematical Modeling and Thermal-hydraulic Analysis of Vertical Water Wall in an Ultra Supercritical Boiler," *Applied Thermal Engineering*, vol. 29, pp. 2500-2507, 2009.

[9] P. J. Edge, P. J. Heggs, M. Pourkashanian, and A. Williams, "An Integrated Computational Fluid Dynamics-process Model of Natural Circulation Steam Generation in a Coal-fired Power Plant," *Computers and Chemical Engineering*, vol. 35, pp. 2618-1631, 2011.

[10] L. G. Shi, "Study of Thermal Performance Calculation Method in Ultra-supercritical Coal Firing Boiler Furnace." M.S. thesis, North China Electric Power University, Baoding, 2008, (in Chinese).

[11] W. Zima, S. Gradziel, and A. Cebula, "Modelling of Heat and Flow Phenomena Occurring in Waterwall Tubes of Boilers for Supercritical Steam Parameters," *Archives of Thermodynamics*, vol. 31, pp. 19-36, 2010.

[12] K. Kitoh, S. Koshizuka, and Y. Oka, "Refinement of Transient Criteria and Safety Analysis for a High-temperature Reactor Cooled by Supercritical Water," Nuclear Technology, vol. 135, pp. 252-264, 2001.

[13] Water & Steam, IAPWS-IF97, Springer-Verlag, 1999.

[14] Q. Y. Fang, H. C. Zhou, H. J. Wang, and T. L. Shi, "Numerical Simulation of the Ash Deposition Characteristics in a W-flame Boiler Furnace," Proceedings of the CSEE, vol. 28, pp. 1-7, 2008, (in Chinese).

[15] D. Zhang, "Numerical Investigation on the Combustion Characteristics of 660 MW W-flame Boiler," M.S. thesis, North China Electric Power University, Baoding, 2009, (in Chinese).

[16] P. J. Smith and L. D. Smoot, "One-dimensional Model for Pulverized Coal Combustion and Gasification," Combustion Science and Technology, vol. 23, pp. 17-31, 1980.

[17] Y. S. Wang, W. D. Fan, L. X. Zhou, and X. C. Xu, *Numerical Calculations of Combustion Process*, Science Press, 1986, (in Chinese).

[18] D. Riechelmann, S. Kato, and T. Fujimori, "Effect of Presumed PDF Selection on the Numerical Result for Turbulent Diffusion Flames,"

JSME, International Journal Series B, vol. 45, pp. 108-111, 2002.

Chen Yang, born in 1963, received Bachelor Degree in Compressor and Refrigeration Technology from Xi'an Jiaotong University and Master Degree and Ph. D from Chongqing University, China. He is currently working as professor in Chongqing University, Chongqing, China.

Hangxing He, born in 1989, received Bachelor Degree in Nuclear Engineering and Technology from Chongqing University, China. He is currently a PhD student in Chongqing University, Chongqing, China.

Li Zhao, born in 1986, received Bachelor and Master Degree in Thermal Energy and Power Engineering from Chongqing University, China. She is currently working in Southwest China Research Institute of Electronic Equipment, Chengdu, China.

Nomenclature

A — flow area, m^2
C_d — drag force coefficient
C_p — specific heat capacity, J/(kg K)
d_{in} — internal diameter, m
d_p — particle diameter, m
g — gravitational acceleration, m/s^2
G — fluid mass flux, $kg/(m^2 s)$
G_w — radiation incident upon the surface, W/m^2
h — specific enthalpy, J/kg
h_c — convective heat transfer coefficient, $W/(m^2 K)$
H_c — heat generated by char combustion, J
H_v — heat precipitation of volatile, J
$\dot{m}$ — mass flow rate, kg/s
m_p — particle mass, kg
m_i — mass precipitation of volatile per kilogram
p — pressure, Pa
$\dot{q}$ — heat flux, W/m^2
$q_{r,w}$ — radiant heat flux, W/m^2
Re — Reynolds number
t — fluid temperature, K
T_f — fluid temperature, K
T_p — particle temperature, K
T_w — wall surface temperature, K
u_p — velocity of coal particle, m/s
z — spatial coordinate, m

Greek symbols

α — heat transfer coefficient, $W/(m^2 K)$
θ — wall temperature, K
ρ — density, kg/m^3
ρ_p — density of coal particle, kg/m^3
ρ_w — reflectivity of the surface
τ — time, s
ε_w — emissivity of the surface
μ — dynamic viscosity, N/(m s)
σ — Stefan-Boltzmann constant
Δt — time step, s
Δz — spatial size of control volume, m